JCTC Journal of Chemical Theory and Computation

Article

pubs.acs.org/JCTC

Fully Internally Contracted Multireference Configuration Interaction Theory Using Density Matrix Renormalization Group: A Reduced-Scaling Implementation Derived by Computer-Aided Tensor Factorization

Masaaki Saitow,[*,†,∥] Yuki Kurashige,[‡,†,§] and Takeshi Yanai[‡,†]

[†]The Graduate University for Advanced Studies, Myodaiji, Okazaki, Aichi 444-8585, Japan

[‡]Department of Theoretical and Computational Molecular Science, Institute for Molecular Science, Okazaki, Aichi 444-8585, Japan

[§]Japan Science and Technology Agency, PRESTO, 4-1-8 Honcho, Kawaguchi, Saitama 332-0012, Japan

Supporting Information

ABSTRACT: We present an extended implementation of the multireference configuration interaction (MRCI) method combined with the quantum-chemical density matrix renormalization group (DMRG). In the previous study, we introduced the combined theory, referred to as DMRG-MRCI, as a method to calculate high-level dynamic electron correlation on top of the DMRG wave function that accounts for active-space (or strong) correlation using a large number of active orbitals. The DMRG-MRCI method is built on the full internal-contraction scheme for the compact reference treatment and on the cumulant approximation for the treatment of the four-particle rank reduced density matrix (4-RDM). The previous implementation achieved the MRCI calculations with the active space (24*e*,24*o*), which are deemed the record largest, whereas the inherent $N_{\mathrm{act}}^{8} \times N$ complexity of computation was found a hindrance to using further large active space. In this study, an extended optimization of the tensor contractions is developed by explicitly incorporating the rank reduction of the decomposed form of the cumulant-approximated 4-RDM into the factorization. It reduces the computational scaling (to $N_{\mathrm{act}}^{7} \times N$) as well as the cache-miss penalty associated with direct evaluation of complex cumulant reconstruction. The present scheme, however, faces the increased complexity of factorization patterns for optimally implementing the tensor contraction terms involving the decomposed 4-RDM objects. We address this complexity using the enhanced symbolic manipulation computer program for deriving and coding programmable equations. The new DMRG-MRCI implementation is applied to the determination of the stability of the iron(IV)-oxo porphyrin relative to the iron(V) electronic isomer (electromer) using the active space (29*e*,29*o*) (including four second d-shell orbitals of iron) with triple-ζ-quality atomic orbital basis sets. The DMRG-cu(4)-MRCI+Q model is shown to favor the triradicaloid iron(IV)-oxo state as the lowest energy state and characterize the iron(V) electromer as thermally inaccessible, supporting the earlier experimental and density functional studies. This conflicts with the previous MR calculations using the restricted active-space second-order perturbation theory (RASPT2) with the similar-size active space (29*e*,28*o*) reported by Pierloot et al. (Radoń, M.; Broclawik, E.; Pierloot, K. *J. Chem. Theory Comput.* **2011**, *7*, 898), showing that the hypothetical iron(V) state indicated by recent laser flash photolysis (LFP) studies is likely thermally accessible because of its underestimated relative energy.

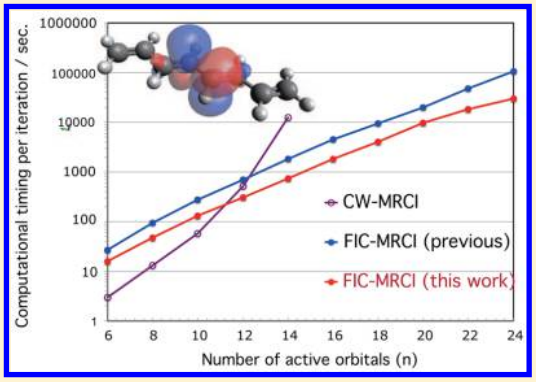

1. INTRODUCTION

The density matrix renormalization group (DMRG) method was introduced by White in 1992 and offered a powerful algorithm for accurately describing properties of quasi-one-dimensional quantum lattice models.[1,2] It was incorporated into the framework of *ab initio* quantum-chemical calculations (*ab initio* DMRG), resulting in an exceedingly efficient alternative to the full configuration interaction (FCI) method to describe highly correlated electronic structures of molecules.[3−41] The drastic reduction in the computational cost in DMRG is ascribed to its compact parametrization of the wave function, known as the matrix product state (MPS).[41−46] The recent technological advances in the quantum-chemical DMRG calculations have revealed that it is capable of overcoming the limitations of conventional multireference (MR) methodologies based on the complete-active-space (CAS) model. By means of the DMRG treatment, the exact diagonalization of the active-space Hamiltonian with approximately 30−40 active molecular orbitals (MOs) is no longer an obstacle for MR calculations. The complete-active-space self-consistent field (CASSCF) scheme[47,48] that uses the DMRG as an engine to

Received: March 21, 2015
Published: September 25, 2015

DOI: 10.1021/acs.jctc.5b00270
J. Chem. Theory Comput. 2015, 11, 5120−5131

diagonalize the active-space Hamiltonian has been proposed by Zgid and Nooijen[16] and by Chan et al.[9] This joint approach combining the DMRG and CASSCF methods, which is referred to as DMRG-CASSCF, has enabled MR calculations for the Mn_4CaO_5 cluster, a catalytic metalloenzyme in photosystem II, using a large active space with 44 electrons in the 35 active MOs,[25] and for several other bioinorganic molecules, such as 2Fe-2S/4Fe-4S clusters,[12,13] nonheme diiron Δ^9 desaturase,[30] and oxo and peroxo dicopper complexes from tyrosinase,[22,29,32] etc.

The DMRG-CASSCF calculations are mainly responsible for the account of static correlation in the CAS framework, while the rest of the correlation, referred to as the *MR dynamic correlation*, is an additional factor to accurately determine energetics of molecular electronic states. In our very recent study,[24] we introduced a method that combines the DMRG-CASSCF reference with the MR configuration interaction (MRCI) method[49−63] and its size-consistency-corrected variants, such as the Davidson's *a posteriori* correction method (MRCI+Q),[64−66] MR averaged coupled-pair functional (MR-ACPF),[67−69] and MR averaged quadratic coupled-cluster (MR-AQCC).[70−73] These integrated methods, referred to as DMRG-MRCI families, were developed as an approach to describe higher level MR dynamic correlation compared to the second-order perturbation (PT2) methods (e.g., CASPT2,[74,75] MCQDPT,[76] and so on). Prior to the development of the DMRG-MRCI methods, we investigated the DMRG-based dynamic correlation methods named DMRG-CASPT2[23,27,29] and DMRG-CT,[31,32] which are the combinations of DMRG with CASPT2[74,75] and canonical transformation (CT)[77,78] theories, respectively. All of these MR dynamic correlation methods have been developed in the full *internal-contraction* (IC) framework that can achieve a compact wave function representation.[24,56,79−83] In addition, the four-particle rank reduced-density matrix (4-RDM) arising in the contracted equations in IC basis was treated in an approximate way using the cumulant reconstruction neglecting higher particle rank cumulants.[24,29] The DMRG-MRCI framework with the cumulant-approximated 4-RDM is referred to as DMRG-cu(4)-MRCI. Very recently, Sharma and Chan presented an alternative approach to DMRG-based PT2 theory by exploiting the space of MPS for the minimization of the PT2 energy.[38]

In the previous study, we demonstrated the feasibility of DMRG-cu(4)-MRCI methods for chemical applications employing long-chain polyenes (up to $C_{24}H_{26}$) and free-base porphyrin as test cases.[24] For these applications, the large active spaces for the full π valence correlation (involving 24 MOs) were successfully treated as CAS reference of the DMRG-cu(4)-MRCI calculations. To implement the DMRG-MRCI methods, we employed a computer-aided approach to derive the working equations consisting of a large number of tensor contraction terms and to translate them into the parallelized and efficiently vectorized computer code. We found that the DMRG-MRCI code derived from the automated generator performs in the $O(N_{act}^8 \times N)$ complexity of computation, where N_{act} means the number of active MOs. Unless otherwise stated, N is used simply to represent the total number of MOs in the system. It should be noted that since our aim is to establish a multireference dynamically correlated method which can deal with a reference function with a large number of active MOs, the exponent of N_{act} dependence in computational scaling serves as the rate-determining index to the overall applicability. This complexity is successfully liberated from the exponential dependence, so that the aforementioned applications were accomplished with a tolerable computational cost. However, the ninth-power dependence of the complexity on N and N_{act} obviously becomes a fundamental hindrance to using DMRG-MRCI for application to further extended systems requiring over 24 active MOs in CAS and several hundreds of virtual MOs.

In this study, we will present an extended implementation of the DMRG-cu(4)-MRCI methods which delivers the scaling reduction from $O(N_{act}^8 \times N)$ to $O(N_{act}^7 \times N)$ in the required floating-point operations. This extension is indispensable for enabling the applications to realistic and challenging chemical problems. For such an application, we attempt to practice the DMRG-MRCI methodology as a highest level MR theory to address an issue being debated on electronic states of iron-oxo porphyrin, known as a chemical species of cytochrome P450 *Compound I* (Cpd I).[84] As reported in earlier studies,[85−88] the MR calculations for this molecule require an extended active space for an ideal treatment because of the nontrivial electronic nature of open-shell Fe core and π-conjugated porphyrin ligand. In order to achieve DMRG-MRCI calculations for the iron-oxo porphyrin, we endeavor to address the aforementioned computational scaling ($O(N_{act}^8 \times N)$) problem in the implementation. For this purpose, the automated generator is extended to handle more complex tensor factorizations and to explicitly account for a cumulant-decomposed form of the 4-RDM[24] (an eight-index tensor); in the previous generator, 4-RDM was simply treated as a single (or undecomposed) tensorial object. The newly extended factorization scheme has been found capable of drastically mitigating high computational demanding in tensor contraction calculations of DMRG-MRCI. In the DMRG-based calculations, we include an extra 4d-type orbital of the iron core in the active space relative to the largest previously reported,[88] leading to the active space with 29 electrons distributed in the 29 active MOs.

This work is organized as follows: In section 2, the general theory and computational implementation of DMRG-MRCI methods are presented. Results and discussion for DMRG study of iron-oxo electromers follow in section 3. Finally, conclusions are drawn in section 4.

2. THEORY

2.1. DMRG-MRCI. We begin with a recapitulation of general algorithmic aspects of the DMRG-MRCI method introduced in our previous study.[24] In the DMRG-MRCI theory, the wave function is written in the full IC (FIC) framework as

$$|\Psi_{MRCI}\rangle := (C_0 + \sum_{pqrs} C_{pq}^{rs} E_{rs}^{ps})|\Psi_0\rangle \quad (1)$$

where $\mathbf{C}$ and $\mathbf{E}$ refer to the MRCI amplitude and the spin-free excitation operator, respectively, while Ψ_0 represents the CAS reference function described by DMRG and CASCI methods. The indices *wxyz*, ..., *ijkl*... and *abcd*... represent the core, active and virtual MOs, respectively, while the others (*prqs*) are used for the generic MOs. Note that E_{pq}^{rs} covers eight types of excitation in total: $co \rightarrow oo$, $cc \rightarrow oo$, $cc \rightarrow ov$, $oo \rightarrow ov$, $cc \rightarrow vv$, $co \rightarrow vv$, $oo \rightarrow vv$, and a combination of $co \rightarrow ov$ and $oc \rightarrow ov$, where the excitation classes are labeled using *c*, *o*, and *v*, referring to core, active and external orbital, respectively. The intra-active excitation (E_{ij}^{kl}) is excluded from the consideration (see ref 24 for details). In eq 1, the action of the *E*-operator to the reference generates the IC basis, an alternative many-body

DOI: 10.1021/acs.jctc.5b00270
J. Chem. Theory Comput. 2015, 11, 5120−5131

basis to the Slater determinant or configuration state function $|e^{rs}_{pq}\rangle \leftarrow E^{ps}_{rs}|\Psi_0\rangle$. Since the IC excitation function is a non-orthonormal and overcomplete basis, the DMRG-MRCI equation takes the form of the generalized eigenvalue equation

$$\mathbf{HC} = \mathbf{SCE} \tag{2}$$

where **H** and **S** represent the Hamiltonian and overlap matrices, respectively. At each step of the block-Davidson procedure[89,90] to solve eq 2, the σ-equation (Hamiltonian matrix−CI vector multiplication) is calculated;

$$\sigma^L = \sum_R \langle e^L|H|e_R\rangle T^R \tag{3}$$

where L (R) refers to either of the eight types of the IC basis and **T** represents the Ritz vector that constitutes the MRCI amplitude (**C** in eq 1). The molecular electronic Hamiltonian in the spin-free formulation is used

$$H = \sum_{pq} h^q_p E^p_q + \frac{1}{2}\sum_{pqrs} V^{rs}_{pq} E^{pq}_{rs} \tag{4}$$

The explicit form of the spin-free working equation is derived from eq 3 and 4 by invoking the normal ordering of the spin-free E-operator.[91] For this purpose, the symbolic manipulation program has been developed by the several groups.[24,31,59,83,92−100] Each term of the MRCI σ-equation is expressed as a product of three tensor objects: amplitude (**T**), molecular integral (**h** or **V** in eq 4), and RDM (**D**). Note that the RDM is an expectation value of the E-operator with respect to the reference function; i.e., $D^{kl\cdots}_{ij\cdots} = \langle\Psi_0|E^{kl\cdots}_{ij\cdots}|\Psi_0\rangle$.

As originally proposed by Werner and Reinsch,[56] when eq 3 is evaluated straightforwardly, the lengthy 5-RDM (a 10-index tensor) arises from the semi-internal excitation (E^{ai}_{jk} and E^{ij}_{kx}) block of the σ-equation, resulting in the significantly large computational scaling of $O(N^{10}_{act} \times (N_{virt} + N_{closed}))$. In our DMRG-MRCI formalism,[24] we evaluate the semi-internal Hamiltonian elements through the commutator relation, for example, for E^{ai}_{jk} excitation operator

$$\sigma^{jk}_{ai} = (\langle\Psi_0|[[E^{jk}_{ai}, H], E^{nb}_{lm}]|\Psi_0\rangle + E_0\langle\Psi_0|E^{jk}_{ai}E^{nb}_{lm}|\Psi_0\rangle)T^{nb}_{lm} \tag{5}$$

where E_0 represents the reference energy. This leads to the elimination of 5-RDM from the programmable equation just as done in the N-electron valence multireference perturbation theory (NEVPT) framework of Angeli et al.[102] It should be noted that the transformation from eq 3 to eq 5 does not utilize any approximation. Validity of eq 5 in the MRCI theory was originally examined by Angeli et al.[103] For this purpose, they reused the third order NEVPT code based on the so-called partial contraction framework, that is essentially equivalent to the FIC framework. As a consequence, the DMRG-MRCI σ-equation can be expressed using only 1−4-RDMs, and then, its computational scaling is reduced to $O(N^8_{act} \times (N_{virt} + N_{core}))$. The proof of this transformation is given in ref 24.

Nevertheless, the eight-index 4-RDM still hinders the application of the DMRG-MRCI to the systems with approximately 20−30 active MOs or more. By neglecting the four-particle rank cumulant in the 4-RDM, the relatively large 4-RDM is decomposed into a sum of an antisymmetrized product of the lower rank RDMs.[104−108] The definition of the cumulant decomposition for the spin-free RDM is not as evident as that in the spin-dependent case.[106−108] Our formulation on the spin-free cumulant-decomposed 4-RDM is given, in the Supporting Information of ref 24, as

$$\begin{aligned} D^{klmn}_{ghij} \rightarrow\ & D^{klm}_{ghi}D^n_j + (15\text{ terms}) \\ & - D^{kl}_{gh}D^{mn}_{ij} + (26\text{ terms}) \\ & + \frac{1}{3}\Gamma^{kl}_{gh}\Gamma^{mn}_{ij} + (26\text{ terms}) \end{aligned} \tag{6}$$

where $\mathbf{\Gamma}$ represents the spin-free cumulant; i.e., $\Gamma^{rs}_{pq} = D^{rs}_{pq} - D^r_p D^s_q + \frac{1}{2}D^s_p D^r_q$.

The full form of the σ-vector (eq 3) and the diagonal preconditioner required in the block-Davidson procedure are composed of approximately as many as 3000 tensor contraction terms in total. The derivation and implementation of such a tremendous amount of terms are somewhat straightforward, but quite prone to errors. To this end, we have developed a tensor generator to expand the many-Fermionic ansatz into the tensor-contracted forms and to translate them to the efficiently vectorized tensor contraction code.[96] The generated program can use more than hundreds of computer nodes on the basis of the message-passing interface (MPI) parallelism.

2.2. Symbolic Optimization of the Cumulant-Approximated 4-RDM. In the previous algorithm implemented in our tensor generator, the largest number of the tensors composing each single-tensor-contraction (TC) term was permitted to be three. This stems from the fact that the most complex form of TC terms in the DMRG-MRCI σ-equation was assumed to be $\sigma \leftarrow \mathbf{V}\cdot\mathbf{T}\cdot\mathbf{D}$, where **V**, **T**, and **D** mean Hamiltonian coefficients (integrals), amplitudes (or CI coefficients), and RDM, respectively. The generator was designed on the basis of this specific TC structure so as to provide optimal factorizations for the efficient evaluation of σ. We have found, however, that this design is a cause that hinders extensibility of the previous code toward a much larger active space, for which the TC terms involving 4-RDM need be evaluated with a formidable number of operation counts. As discussed earlier, the previous study introduced the rank reduction of 4-RDM using cumulant approximation, which offered a significant memory saving for σ. If the cumulant decomposition of 4-RDM (eq 6) is explicitly considered in expressing the σ-equation, the terms involving the 4-RDM for **D** take an extended form as $\sigma \leftarrow \mathbf{V}\cdot\mathbf{T}\cdot\mathbf{D}_m\cdot\mathbf{D}_{(4-m)}$ (which involves four tensor objects), where m refers to the particle rank of the RDM and is either of 1, 2, or 3. Because the previous code generator was incapable of factorizing TC with more than three tensors, the decomposed form of 4-RDM was not explicitly used in the process of TC factorization; in fact, the approximate 4-RDM was treated as a single (or undecomposed) eight-index tensor $\mathbf{D}_4$, so that the number of tensors in each TC term did not exceed 3. In the resulting scheme, the cumulant reconstruction of the 4-RDM and associated tensor contraction require the floating-point operations (FPOs) of $O(N^8_{act})$ and $O(N^8_{act} \times N)$, respectively, which are the most demanding part of the σ-vector calculation. In addition, the $O(N^8_{act})$ operations for the cumulant reconstruction cannot be efficiently vectorized because of its direct-product nature, to which high-performance matrix multiplication subroutines, such as DGEMM, is inapplicable. For the systems with approximately 30 active MOs, it was found that the unvectorized $O(N^8_{act})$ manipulation causes a substantial cache-miss penalty.

In this study, we have extended the generator to achieve an extraoptimization of code for the TC involving 4-RDM. The

DOI: 10.1021/acs.jctc.5b00270
J. Chem. Theory Comput. 2015, 11, 5120−5131

key for the optimization lies in a more complicated factorization to exploit the decomposed form of the cumulant-approximated 4-RDM. As an extension, we have newly developed a symbolic program that can deal with the factorization of TC terms with an arbitrary number of tensor factors. The symbolic manipulation part of our tensor generator has been redesigned so as to further minimize the FPO and to eliminate the unvectorized step. The new algorithm factorizes the TC terms into a cascaded stream of binary TCs, and the optimal factorization is derived by taking into account all possible patterns of binary contraction forms. The computer program, which is written in Haskell language[109] allowing the purely functional programming, is readily capable of optimizing the binary TCs with respect to minimization of FPO in the presence of permutation symmetry of tensors. The generated code is parallelized with MPI on a memory distributed computer system. As a consequence, the formal scaling of the DMRG-MRCI is reduced from $O(N_{\mathrm{act}}^8 \times N)$ to $O(N_{\mathrm{act}}^7 \times N)$. In addition, the unvectorized $O(N_{\mathrm{act}}^8)$ expense for the cumulant reconstruction of the 4-RDM is eliminated from the construction of the σ-equation; this means that the associated cache-miss penalty is reduced.

For a fairly large system, it was also observed that the sorting of each tensor in the binary contraction, as a preprocess to perform the central matrix−matrix multiplication, may become crucial. The index sorting algorithm often causes a drastic amount of cache-miss, leading to an extreme degradation in computational throughput. An optimization algorithm for the presorting of the tensor indices has been implemented in the code generator. Due to these modifications, the new DMRG-MRCI program shows a drastic speedup relative to the previous version and is routinely applicable even to the systems with more than 30 active MOs.

Hereafter, we briefly sketch the basic design of our tensor contraction program used for the construction of the σ-vector. Since our target is execution of the DMRG-MRCI for the systems with approximately 60 closed, 30 active, and 500 virtual MOs, loop-fusion among the binary contractions is a necessary requirement to reduce the size of the intermediate arrays that should be allocated on the fast memory. If the term has only three tensor factors, the term is decomposed into two binary contractions and there are only three possibilities to form them: $((\mathbf{V}\cdot\mathbf{D})\cdot\mathbf{T})$, $((\mathbf{V}\cdot\mathbf{T})\cdot\mathbf{D})$, and $((\mathbf{D}\cdot\mathbf{T})\cdot\mathbf{V})$. In this case, factorization of the term into the binary contraction and fusion of the loops shared with both binary contractions are rather simple. However, if the number of the tensor factors is 4, the number of the unique combinations to form the binary contractions is as many as 15.[110] Among them, 12 patterns form the *sequential* contractions, i.e., for instance $(((\mathbf{V}\cdot\mathbf{D}_m)\cdot\mathbf{T})\cdot\mathbf{D}_{(4-m)})$, while the remaining three are the *nonsequential* contraction patterns such as $((\mathbf{V}\cdot\mathbf{D}_m)\cdot(\mathbf{T}\cdot\mathbf{D}_{(4-m)}))$. The algorithm to fuse the common loops among the binary contractions also becomes much more complicated than that for the loop-fusion of the two binary contractions. The so-called "purely functional" programming model, on which Haskell language is based, allows one to quickly and safely implement complicated optimization algorithm into computer code: This would be one of the primal reasons for which Haskell is particularly used in the field of financial engineering such as high-frequency trading of financial commodities.[111]

3. RESULTS AND DISCUSSION

3.1. Efficiency Test for DMRG-MRCI Code. To estimate the efficiency of the current FIC-MRCI implementation, we have performed a benchmark calculation on the $[H_4Fe_2O_7]^{2+}$, a hypothetical diferrate intermediate that catalyzes the water to form the O−O bond,[112] using ANO-RCC basis set. Reference 112 details the multireference description of the water splitting reaction mediated by this compound. The diferrate system is composed of 19 closed, 32 active, and 279 virtual orbitals. The active space is constructed as follows: (1) we have added all five 3d orbitals of two Fe atoms, (2) all of the valence 2p and double-shell 2p′ orbitals of two adjacent O atoms, and two 2p orbitals of the remaining five O atoms into active space. This active-space setting results in 36 electrons distributed in 32 active orbitals (=5 × 2 + [3 + 3] × 2 + 2× 5). The calculation was performed on top of a MPI-based parallelization using six computer nodes; each of which has two hexacore Intel Xeon X5660 processors of 2.80 GHz and 96 gigabytes of memory. As preliminary steps to diagonalize the DMRG-MRCI Hamiltonian, two intermediate tensors [$\mathbf{\Gamma}_\mathbf{A}$ and $\mathbf{\Gamma}_\mathbf{B}$ in ref 24] have to be constructed whose associated tensor contraction require FPOs of $O(N_{\mathrm{act}}^8)$ and $O(N_{\mathrm{act}}^8 \times (N_{\mathrm{virt}} + N_{\mathrm{act}} + N_{\mathrm{closed}}))$, respectively. Both $\mathbf{\Gamma}_\mathbf{A}$ and $\mathbf{\Gamma}_\mathbf{B}$ are formed by contracting the 4-RDM and electron repulsion integral ($\mathbf{V}$ in eq 4) as

$$(\Gamma_{\mathrm{A}})_{gh}^{kl} \leftarrow \sum_{ijmn} D_{ghij}^{klmn} V_{mn}^{ij} \tag{7}$$

$$(\Gamma_{\mathrm{B}})_{ghp}^{klm} \leftarrow \sum_{ijn} D_{ghij}^{klmn} V_{pn}^{ij} \tag{8}$$

By using the previous DMRG-MRCI code, the noniterative construction of $\mathbf{\Gamma}_\mathbf{A}$ and $\mathbf{\Gamma}_\mathbf{B}$ were observed to take 4,311 and 1,141,585 s, respectively, in wall time. In the current implementation, the 4-RDM in both eqs 7 and 8 is explicitly decomposed into the cumulant-approximation and factorized into binary tensor contractions. Because of this, the largest FPOs for construction of $\mathbf{\Gamma}_\mathbf{A}$ and $\mathbf{\Gamma}_\mathbf{B}$ are reduced from $O(N_{\mathrm{act}}^8)$ and $O(N_{\mathrm{act}}^8 \times (N_{\mathrm{virt}} + N_{\mathrm{act}} + N_{\mathrm{closed}}))$ to $O(N_{\mathrm{act}}^7)$ and $O(N_{\mathrm{act}}^7 \times (N_{\mathrm{virt}} + N_{\mathrm{act}} + N_{\mathrm{closed}}))$, respectively. In the current implementation, constructions of the $\mathbf{\Gamma}_\mathbf{A}$ and $\mathbf{\Gamma}_\mathbf{B}$ were observed to take 16 and 1,569 s, respectively, in wall time on the same cluster configuration. Note that these steps come prior to the Davidson iteration and should be performed only once in a single DMRG-MRCI calculation. Owing to the explicit decomposition of the 4-RDM in the σ-equation (eq 3), the computational scaling is reduced to $O(N_{\mathrm{act}}^7 \times N)$ from the previous one ($O(N_{\mathrm{act}}^8 \times N)$). The actual computational timings for a single σ-vector evaluated with the previous and current implementations were measured to be 869,959 and 125,095 s, respectively, in wall time. As a consequence of the reduction in the computational scaling and of the elimination of the unvectorized cumulant reconstruction, a drastic acceleration was achieved in the construction of both the σ-vector and the preliminary intermediates.

To estimate the computational accelerations of the current improvements, we have further performed a benchmark calculation for a set of linear polyene chains (C_6H_8 − $C_{24}H_{26}$). The 1s orbitals of H and C atoms were treated as frozen core while all of the out-of-plane $2p_z$ (π) orbitals of C atom as active orbitals; this MO composition leads to use of CAS(ne, no) for C_nH_{n+2} molecule. The 6-31G* basis set was used and the C_{2h} spatial symmetry was fully exploited to reduce

DOI: 10.1021/acs.jctc.5b00270
J. Chem. Theory Comput. 2015, 11, 5120−5131

the amount of the required storage and the total FPOs. The partial internally contracted MRCI code[59] that is based on the Celani–Werner (CW)-type contraction scheme[113,114] was used as a reference to the conventional implementation whose computational scaling increases exponentially with respect to the molecular size ($\approx O(e^N)$). For the FIC-MRCI calculations, the three cluster nodes were used with the same hardware specification to the previous case. To the best of our knowledge, only the serial version of the CW-MRCI code is commercially available. Therefore, the CW-MRCI calculations were performed on a single node of the cluster by using the Molpro program suite of version 2012.1.[115]

The computational timings per a single Davidson iteration are given in Figure 1 and Table 1 for previous and current implementations of the FIC-MRCI. For C_6H_6, which is a smallest molecule in the benchmark set, the speedup ratio caused by the new factorization algorithm is merely up to 1.69. As the size of the molecule becomes larger, it is recognized that the computational time of the new FIC-MRCI implementation is less than half of the previous one, achieving the speedup ratio up to 2.61 for $C_{18}H_{20}$. For $C_{24}H_{26}$, the new implementation is observed to be extremely efficient and is approximately 3.5 times faster than the previous one. This suggests that, for the molecules which involve more than 24 active MOs, the cumulant reconstruction of the 4-RDM readily dominates the total computational time. For relatively small molecules with less than 14 active MOs, The CW-MRCI scheme (Molpro) still performs quite well and is more than five times faster than our new FIC-MRCI implementation. Nevertheless, its computational time grows exponentially with respect to the size of the polyene chain due to the fact that the semi-internal excitation configurations are uncontracted in the wave function ansatz.

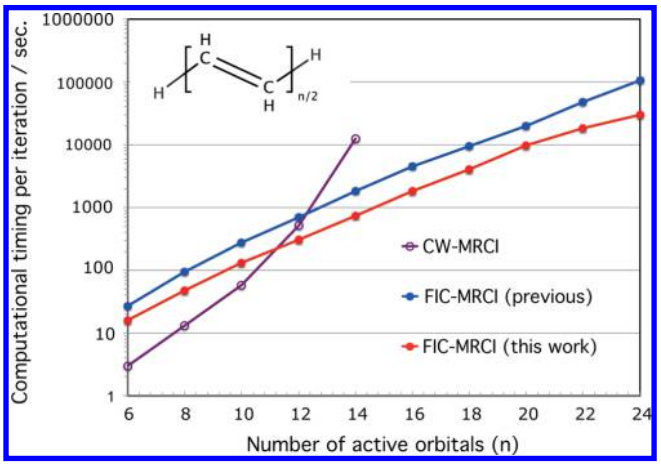

Figure 1. Computational timing per a single iteration of the previous and current FIC-MRCI implementations for linear polyene chains ranging from C_6H_6 to $C_{24}H_{24}$. All of the $2p_z$ orbitals of C atom were included in the active space. The 1s orbitals of H and C atoms were set as frozen. For comparison, the timing data of the CW-MRCI (based on the partially contracted scheme) are also given.[59]

Table 1. Calculation Times for Construction of a Single σ Vector of the Previous and Current FIC-MRCI Implementations for C_nH_{n+2} ($6 \le n \le 24$) with the CAS(ne,no) Reference[a]

		FIC-MRCI		
molecule	CW-MRCI	previous	current	speedup ratio
C_6H_8	3	27	16	1.69
C_8H_{10}	13	94	47	2.00
$C_{10}H_{12}$	58	277	131	2.11
$C_{12}H_{14}$	515	698	304	2.30
$C_{14}H_{16}$	12424	1805	730	2.47
$C_{16}H_{18}$		4572	1818	2.51
$C_{18}H_{20}$		9566	4030	2.37
$C_{20}H_{22}$		19584	9719	2.02
$C_{22}H_{24}$		47340	18132	2.61
$C_{24}H_{26}$		104396	30142	3.46

[a]All timings are given in seconds. All out-of-plane valence 2p orbitals were included in the CAS. All 1s orbitals of C and H were kept uncorrelated.

3.2. Relative Stability of FeO(P)Cl Electromers. We now turn to the application of the DMRG-MRCI method for the determination of relative energies of iron-oxo porphyrin electromers. Cytochrome P450 is a large superfamily of protein-bound porphyrin complexes with coordination of an active oxygen that hydroxylates the substrate. Due to the highly active nature of the ligand oxygen, the cytochrome P450 catalyzes conversion of a variety of chemical compounds by inserting the oxygen atom into an inert C–H bond of the substrate.[116,117] The reactive intermediate in the cytochrome P450 catalytic reaction is postulated to be an iron(IV)-oxo porphyrin radical cation, which is often referred to (or widely accepted) as Cpd I[84] and is considered to participate in oxygen-transfer reaction.[118] While neutral iron(III)-oxo porphyrin derivatives are relatively inert, a more oxidized iron(IV)-oxo porphyrin radical cation is known to be a highly reactive oxidant in an *in vivo* context, which is ascribed to the extremely electrophilic nature of the Fe^{IV}–O group. On the basis of spectroscopic studies using various experimental techniques,[119−124] the electronic character of the iron-oxo group in enzymatic Cpd I species and their analogues was confirmed to be triradicaloid iron(IV)-oxo for the ground state. This observation was justified by theoretical means, mainly based on the density functional theory (DFT).[84] In this sense, a consensus has been thought to be established between theory and experiment. Stability of this highly oxidized state of iron(IV) is provided by the coordination of porphyrin and oxo ligand, which are both regarded as strong donors.

Meanwhile, recent advances in the laser flash photolysis (LFP) technique have suggested the existence of a low-lying and thermally accessible iron(V)-oxo porphyrin electronic isomer (electromer).[125,126] The iron(V)-oxo group was indeed spectroscopically detected in real time in a synthetic complex with the corrole ligand;[127] this accessibility to Fe^V can be understood from the corrole ligand being a much stronger electron donor than the porphyrin. Stabilization of the (+V) oxidation state of iron was also observed under the presence of the other strong electron donor in several iron-oxo compounds.[128,129] Therefore, it may be plausible for the thermally accessible iron(V)-oxo compounds with the porphyrin ligand to really exist in the biological context. It was reported that the synthetic iron(V)-oxo porphyrin transient reacts 4–5 orders of magnitude faster than the corresponding iron(IV)-oxo electromers.[130] If the iron(V)-oxo species are identified to be another accessible intermediate in an *in vivo* enzymatic cycle, the established chemical picture needs be reconsidered because of its potential role as a remarkably strong oxidant.

DOI: 10.1021/acs.jctc.5b00270
J. Chem. Theory Comput. 2015, 11, 5120−5131

Shaik et al. theoretically showed, by performing MR *ab initio* wave function calculations on the enzymes $P450_{cam}$ and chloroperoxidase (CPO), that the hypothetical iron(V)-oxo states lie at relatively low energies. Although the iron(IV)-oxo state was confirmed to remain the lowest lying, it was suggested that the iron(V)-oxo electromer is possibly accessible.[86] In the study, the CASPT2 level of theory with the reference wave function built with 15 active electrons distributed to 14 active orbitals, denoted (15*e*,14*o*), was employed for electron correlation treatment in conjunction with peripheral modeling based on the molecular mechanics.

Soon after, Pierloot et al. assessed the relative stability of the iron(V)-oxo electromer for two heme complexes, $FeO(P)^+$ and FeO(P)Cl (P = porphyrin), using extended MR active spaces with the CASPT2 method [(15*e*,16*o*)] as well as the restricted active-space second-order perturbation (RASPT2)[131] method [(29*e*,28*o*)], along with a number of DFT methods.[88] In the RASPT2 calculations, the 28 active orbitals consisted of 16 π MOs of the porphyrin, all of the 3d orbitals of iron, 2p orbitals of oxygen, and a further three d-type MOs associated with the 4d shell, and a sufficiently large basis set was used. Using CASPT2 with the (15*e*,16*o*) reference, which is somewhat larger than that used by Shaik et al., the iron(V)-oxo states were found at low energy, as was previously predicted. Pierloot et al. then introduced a much extended active space [(29*e*,28*o*)] because the modest CAS setting was suspected to cause the overstabilization of the iron(V)-oxo states in the multireference PT2 calculations. As it turns out, however, the RASPT2-(29*e*,28*o*) treatment stabilized the iron(V)-oxo porphyrin even more for the studied heme complexes *in vacuo*, and the iron(V)-oxo state was again predicted to be the ground state (i.e., more stable than the iron(IV)-oxo electromer). The RASPT2 description based on the large active space is thus contradictory to the consensus early established by experimental and theoretical (DFT) studies. In the study, the error of the RASPT2 prediction was then speculated to arise from environmental effects. In the presence of the polarizable continuum, it was indeed observed with the DFT-level calculations that iron(IV)-oxo porphyrin was more greatly stabilized relative to the iron(V)-oxo electromer.

In order to provide a more complete picture to determine the relative stability of the iron(IV)-oxo versus iron(V)-oxo electromers, the following requirements for theoretical treatments would ideally have to be fulfilled: (1) MR characterization would need to use a large active space that can cover full-valence correlation space arising from π conjugation of porphyrin moiety and Fe ion including its 4d shell. (2) The CAS model[132−134] would be used rather than the RAS analogue. The CAS framework is based on the FCI expansion of active-space wave function, alternatively referred to as CASCI, while the RAS analogue involves extra partitioning of active orbitals and partly exploits truncated CI that restricts the correlation level depending on the partitioned sets of active orbitals. (3) There would need to be high-level treatment of dynamic correlation beyond the second-order perturbation level of theory. The computational effort of the CASCI method explicitly depends on the dimension of the Hilbert space and thus scales exponentially with respect to the size of the molecule. Therefore, the applicability of the traditional CAS methods is limited to the active space with, for instance, 16 electrons distributed in the 16 MOs. Note that numerous attempts to overcome this limitation have been made, e.g., RAS method,[135,136] general multiconfiguration (GMC) method,[137] generalized valence bond (GVB) method,[138] and perfect pairing and other valence-bond, geminal-type theories,[139−144] generalized active space (GAS) with splitGAS model,[145] the occupation-restricted-multiple-active-space (ORMAS),[146] active-space decomposition methods,[147] and countless others. Here, we attempt to ascertain the stability of the hypothetical iron(V)-oxo electromer of the Cpd I by means of the high-level multireference theory with the DMRG-MRCI and DMRG-CASPT2 models.

As a model molecule for the active intermediate of the Cpd I, we investigated neutral FeO(P) (Cl) where P stands for porphin. This molecule was considered in the previous work of Pierloot et al.[88] Following the work, we focused on the three most relevant electronic states, labeled as $^4A_2$, $^6A_1$, and ^2E, respectively (given under C_{4v} symmetry). The $^4A_2$ state has a triradicaloid character associated with a triplet tetravalent iron, denoted $^3Fe^{IV}$, under the presence of the cationic porphyrin moiety $^2P^{\bullet+}$. From the earlier DFT and experimental results, it has been long considered to be the ground state. The $^6A_1$ state is a high-spin pentaradicaloid, involving a local quintet state on iron-oxo, denoted $^5Fe^{IV}$, which is ferromagnetically coupled with the radical cation $^2P^{\bullet+}$. Note that in the work of Pierloot et al., the large-scale RASPT2 predicted $^6A_1$ electromer was more stable than the $^4A_2$ state, leading to additional contradiction to the experimental consensus. As described earlier, the recent LFP measurement[127−130] and CASPT2/RASPT2 calculations[86,88] indicated the accessibility to an electromer arising from the further oxidized iron-oxo group $^2Fe^{V}O$. This electronic state corresponds to ^2E, involving closed-shell ^1P.

We performed the DMRG-based MR calculations on these three states. The same geometries were used as in ref 88; they were obtained using DFT with the BP86 functional[148,149] for individual states. We assume that the *z* axis is aligned with the linear O−Fe−Cl bond, and the *x* and *y* axes are oriented as shown in Figure 2. Our calculations employed the ANO-RCC

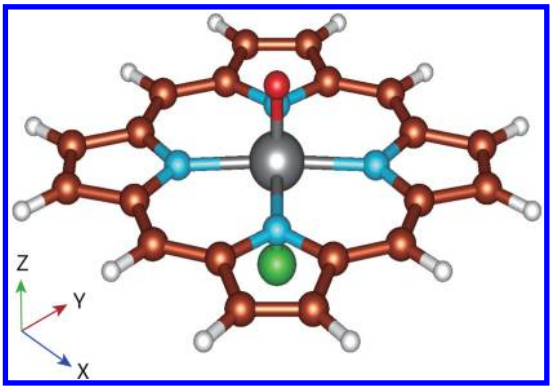

Figure 2. Computational coordination of the FeO(P)Cl molecule. The *z* axis is aligned along the O−Fe−Cl bond while the *x* and *y* axes bisect the N−Fe−N angle.

basis sets[150] with two types of contractions, denoted BS1 and BS2. The contractions for the Fe and O atoms are each common to BS1 and BS2, Fe[7s6p5d3f2g1h] and O[4s3p2d1f], while those for the remaining atoms are given differently for BS1 and BS2, as (BS1) H[2s], C[3s2p1d], N[3s2p1d], and Cl[4s3p1d] and (BS2) H[3s1p], C[4s3p2d1f], N[4s3p2d1f], and Cl[5s4p3d2f]. Note that BS2 is equivalent to the basis set referred to as "basis II" in ref 88. Scalar-relativistic effects were taken into account at the second-order Douglas−Kroll−Hess (DKH2) level of theory.[151,152] Our computer implementation

DOI: 10.1021/acs.jctc.5b00270
J. Chem. Theory Comput. 2015, 11, 5120−5131

is limited to the Abelian group, so that the C_{2v} point-group symmetry was actually used as a subgroup of C_{4v}.

In our MR calculations, the reference wave functions were determined using the DMRG-CASSCF method[9,16] with the active space (29*e*,29*o*). This active space encompasses that used in the previous RASPT2 calculations, (29*e*,28*o*).[88] The previous 28 active orbitals come from five metal 3d, three double-shell metal d orbitals (designated 3d′), the oxygen 2p, 16 of the π/π^* orbitals from N and C in the porphyrin ring (excluding the eight C's farthest from the metal), and the orbital arising from the highest energy combination of four N σ pairs. In addition to them, Fe $3d'_{z^2}$ was newly included in our active space as another double-shell d orbital. The shapes of the active orbitals are shown in the Supporting Information (Figure S4) along with their ordering assigned to the one-dimensional lattice in the DMRG calculations. In the case of the iron(IV)-oxo electromer, the active electrons can be derived from the following model configuration: $3d^4 4s^0$ for Fe(IV), $2p^6$ for O, tweleve $2p_z^1$ for C as well as two $2p_z^1$, two $2p_z^2$, and $2p_\sigma^2$ for N with one electron taken away from P. The active-space DMRG wave functions were calculated with M = 1024 spin-adapted many-electron renormalized basis functions. The initial superblock configurations were set manually in a manner such that the state with the desired multiplicity was allowed to be constructed in the earliest DMRG sweep step.

On top of the reference DMRG-CASSCF descriptions, we computed dynamic correlation using the DMRG-cu(4)-MRCI method[24] with and without Pople's size-consistency correction, denoted +Q(PC).[66] The DMRG-cu(4)-MRCI calculations employed the overlap truncation with the threshold of $\tau = 10^{-2}$ (see also ref 24 for the definition of τ). Note that this value was the smallest that could provide convergence of the iterative MRCI solution, and it produced the DMRG-cu(4)-MRCI relative energies with an error of 6% compared to those obtained with $\tau = 2 \times 10^{-2}$. In addition, the DMRG-cu(4)-CASPT2[23,27,29] calculations were carried out employing the zero-order Hamiltonian modified with the ionization potential/electron affinity (IPEA)[153] specified to be 0.25 au and an imaginary denominator shift (IS)[154] of 0.2 au. The BS1 and BS2 basis sets were used for DMRG-cu(4)-CASPT2 calculations. For DMRG-cu(4)-MRCI calculations, only BS1 (508 functions) was used because BS2 (968 functions) was too demanding. The energies of the DMRG-cu(4)-MRCI method with BS2 ($E_{\text{DMRG-cu(4)-MRCI/BS2}}$) were estimated by the extrapolation given as $E_{\text{DMRG-cu(4)-MRCI/BS2}} = E_{\text{DMRG-cu(4)-MRCI/BS1}} + (E_{\text{DMRG-cu(4)-CASPT2/BS2}} - E_{\text{DMRG-cu(4)-CASPT2/BS1}})$. The DMRG calculations were performed with the orz package, our in-house quantum chemistry program suite.

Figure 3 is a plot of the natural orbitals (NOs) containing iron d orbitals, which were obtained with the DMRG-CASSCF calculations. It includes the porphyrin π orbitals (π (P)), on which the radical with the a_{2u}-type hole is formed for the $^4A_2$ and $^6A_1$ states. Note that the double-shell orbital $3d'_{z^2}$ was not included in the active space of Pierloot et al. The rest of the NOs in the active space are plotted in Supporting Information Figures S1−S3. Table 2 shows the occupancies of the NOs with the orbital nature, $3d_{x^2-y^2}$, π (P), π^*_{xz} (Fe−O), π^*_{yz} (Fe−O), σ^*_{xy} (Fe−P), and $\sigma^*_{z^2}$ (Fe−O), plotted in Figure 3. These calculated occupancies reveal the presence of singly occupied orbitals, clearly representing triradical, pentaradical, and monoradical characters for the $^4A_2$, $^6A_1$, and ^2E states, respectively. For the ^2E state, the π^*_{xz} (Fe−O) orbital is solely singly occupied. For the triradicaloid $^4A_2$ state, there are three singly occupied

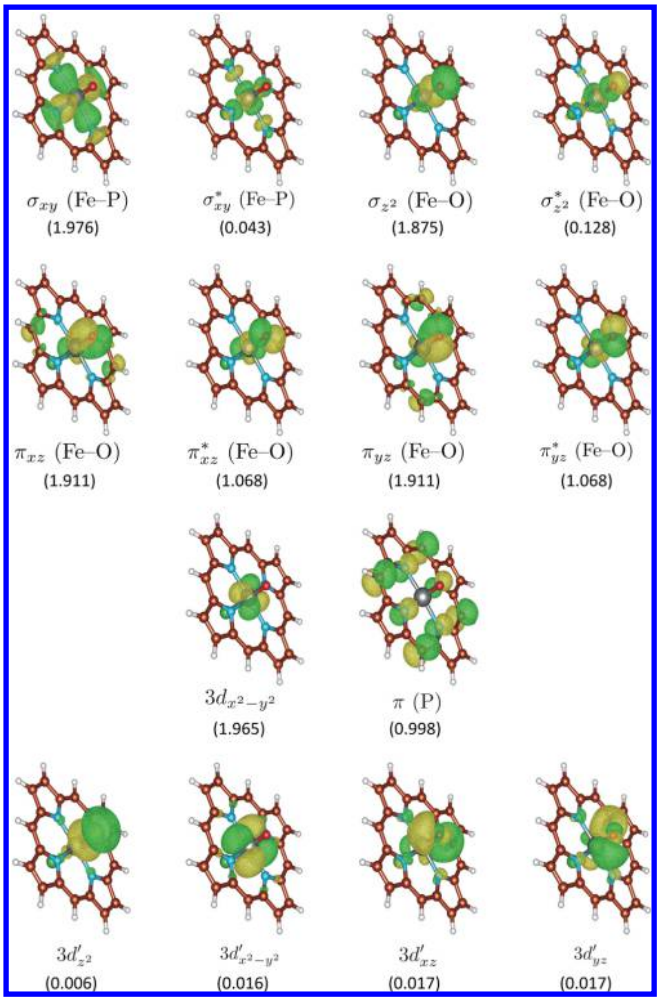

Figure 3. Natural orbitals (NOs) resulting from DMRG-CASSCF-(29*e*,29*o*) calculation for the $^4A_2$ state. The occupation number for each NO is shown in parentheses. These MOs were depicted by using the Charmol, a program for molecular graphics (http://sourceforge.net/projects/charmol/).

orbitals arising from the antibonding orbitals π^*_{xz} (Fe−O) and π^*_{yz} (Fe−O), and the highest occupied π (P) orbital in the porphyrin (see Figure 1 of ref 88). The pentaradicaloid $^6A_1$ state is regarded as formed by local excitation on Fe^{IV} relative to the triradicaloid $^4A_2$ state where a local spin promotion takes place from the nonbonding $3d_{x^2-y^2}$ orbital to the σ^*_{xy} (Fe−P). The electronic configurations based on these NO pictures from the DMRG-CASSCF wave functions are consistent with those shown in the previous studies.

Now we discuss the relative stability of the three electromers. Table 3 displays their relative adiabatic energies obtained with the DMRG-based MR calculations. For comparison, it includes the DFT, CASPT2(15*e*,16*o*), and RASPT2(29*e*,28*o*) results reported in the study of Pierloot et al.[88] The relative energies are given with respect to $^4A_2$. As described in ref 88, the DFT results were strongly functional-dependent, showing that the hybrid functionals, B3LYP and B3LYP*, favor the $^4A_2$ state, but in contrast the pure functionals, OLYP and BP86, give positive but small relative energies for ^2E state. We focus on the DMRG results obtained with the BS2 basis set. First, the energetics of the tetravalent (Fe^{IV}) electromers is discussed, i.e., $^4A_2$ versus $^6A_1$. The DMRG-cu(4)-CASPT2 and DMRG-cu(4)-MRCI results all predicted that the low-spin state ($^4A_2$)

DOI: 10.1021/acs.jctc.5b00270
J. Chem. Theory Comput. 2015, 11, 5120−5131

Table 2. Occupation Numbers of the Open-Shell Orbitals for the Iron-Oxo Porphyrin Electromers Obtained by the DMRG-CASSCF(28*e*,29*o*) Orbital Optimization

	$3d_{x^2-y^2}$	π (P)	π^*_{xz} (Fe−O)	π^*_{yz} (Fe−O)	σ^*_{xy} (Fe−P)	$\sigma^*_{z^2}$ (Fe−O)
$^4A_2$	1.965	0.998	1.068	1.068	0.043	0.128
$^6A_1$	0.996	0.997	1.051	1.051	1.004	0.116
^2E	1.964	1.863	1.061	1.946	0.066	0.231

Table 3. Relative Energies (kcal/mol) of Low-Lying Electronic States of FeO(P)(Cl)

	$(^3Fe^{IV}O)(^2P^{\bullet+})$	$(^5Fe^{IV}O)(^2P^{\bullet+})$	$(^2Fe^{V}O)(^1P)$
method	$^4A_2$	$^6A_1$	^2E
BS1 (508 functions)			
DMRG-CASSCF	0	−8.64	30.22
DMRG-cu(4)-CASPT2	0	1.41	4.52
DMRG-cu(4)-MRCI	0	−0.59	23.84
DMRG-cu(4)-MRCI+Q(PC)	0	4.99	11.87
BS2 (968 functions)			
CASPT2(15*e*,16*o*)[a]	0	3.2	1.6
RASPT2(29*e*,28*o*)[a]	0	−1.5	−1.7
DMRG-CASSCF	0	−5.14	27.70
DMRG-cu(4)-CASPT2	0	3.06	−0.33
DMRG-cu(4)-MRCI[b]	0	1.05	18.99
DMRG-cu(4)-MRCI+Q(PC)[b]	0	6.64	7.01
B3LYP[a]	0	9.7	12.4
B3LYP*[a]	0	12.9	13.30
OLYP[a]	0	10.1	2.9
BP86[a]	0	19.1	1.0

[a]From ref 88. DFT def2-TZVP. [b]Extrapolated.

is more stable than the high-spin state ($^6A_1$) with a relatively small energy gap (1.05−3.42 kcal/mol). The DMRG-cu(4)-MRCI+Q(PC) also favors $^4A_2$ as a more stable state with an energy difference of 6.64 kcal/mol relative to $^6A_1$, which is slightly overestimated compared to the other DMRG results. Pierloot et al. showed that the CASPT2 and RASPT2 calculations may somewhat overestimate the stability of the high-spin pentaradicaloid form of the iron(IV)-oxo electromer on the basis of the comparison with the coupled cluster calculations as well as preceding experiences.

In the previous study,[88] the hypothetical iron(V)-oxo electromer (^2E) was shown from the CASPT2(15*e*,16*o*) and RASPT2 (29*e*,28*o*) calculations to be at low energy and closely lying to the energy level of the iron(IV)-oxo counterparts; therefore, the thermal accessibility to Fe^V was indicated to be likely. Note that the active space for the CASPT2 calculations, (15*e*,16*o*), was based on the four porphyrin π orbitals. In accordance with these results, the present calculations at the DMRG-cu(4)-CASPT2 level of theory with large active space predicted that ^2E and $^4A_2$ are near degenerate with a relative energy of −0.33 kcal/mol. Pierloot et al. evinced that RASPT2 and CCSD(T) closely agree on the relative stability of the Fe(V)-oxo and Fe(IV)-oxo electromers for the simplified heme-like model. However, as shown in Table 3, this stability of the ^2E state was not confirmed at the DMRG-MRCI levels of theory. The ^2E state was estimated to be an excited state lying at 18.99 and 7.01 kcal/mol above the $^4A_2$ state by the DMRG-cu(4)-MRCI and DMRG-cu(4)-MRCI+Q(PC) methods, respectively; these relative energies are much higher than the CASPT2-based relative energies. Roughly speaking, the relative stability of ^2E determined with the DMRG-MRCI families coincides with the DFT results with hybrid functionals. Note that the +Q correction in general cannot perfectly rectify the size-consistency error. The assessment of the size-consistency error of the MRCI methods is demonstrated using polyene supersystems in the Supporting Information. The Pople formula [+Q(PC)] is deemed to have a close resemblance to the energy functional of the MR-ACPF, vanishing for two-electron systems where MRCISD gives the FCI energy. In addition, Krisiloff and Carter have demonstrated that MRCI+Q(PC) gives quite similar correlation energies even for fairly large systems up to $C_{50}H_{52}$;[55] This suggests that the DMRG-cu(4)-MRCI+Q(PC) energy should be intimately comparable to the MR-ACPF energy. The MRCI methodologies are a more sophisticated approach than CAS/RASPT2, involving higher order dynamic correlation as demonstrated in ref 59 by construction. Therefore, it is adequate to conclude that the MRCI+Q result is more reliable than those of previous RAS/CASPT2. All of the DFT methods suggest that the $^4A_2$ is the lowest, in accordance with the MRCI, while the relative energies vary depending on the choice of the functional. It should be mentioned that it is not straightforward to compare the MRCI results with those of DFT methodologies from a theoretical point of view. Overall, the DMRG-MRCI+Q(PC) method, which is capable of accounting for higher level electron correlation than DMRG-CASPT2, substantially favors the $^4A_2$ state (triradicaloid iron(IV)-oxo) as the lowest energy state, supporting the earlier DFT and experimental studies. As a consequence, our theoretical examination based on the DMRG-MRCI methods does not support the thermal accessibility to the hypothetical iron(V)-oxo electromer (^2E) because of its estimated relative energy (+7 kcal/mol or higher). Additionally, it is noted that Pierloot et al. showed that the presence of environment effects serves as further stabilizing $^4A_2$ and destabilizing ^2E.[88]

DOI: 10.1021/acs.jctc.5b00270
J. Chem. Theory Comput. 2015, 11, 5120−5131

4. CONCLUDING REMARKS

We have developed the extended DMRG-cu(4)-MRCI implementation to make possible the application of further large-size MR systems (requiring more than 24 active orbitals for the reference space). In the extension, the rank reduction in the cumulant-approximated 4-RDM has been exploited in the factorization of the tensor contraction terms. This rose the complexity of the factorization patterns in deriving programmable equations, while the enhanced symbolic manipulation program, written in Haskell purely functional programming language, was capable of dealing with it to derive an optimal factorization. The factorized equations are then translated into the parallelized and efficiently vectorized computer code. In the resultant implementation, a drastic reduction has been achieved in the complexity of computation from $N_{act}^{8} \times N$ to $N_{act}^{7} \times N$ along with the elimination of the cache-miss penalty associated with the "direct" cumulant reconstruction that was carried out in the previous implementation. The excellent acceleration was demonstrated in the illustrative benchmark calculations performed on the diferrate intermediate $[H_4Fe_2O_7]^{2+}$ using 32 active orbitals (beyond the previous limitation) and on the polyenes $C_{2n}H_{2n+2}$ using $2n$ active orbitals for n = 3, ..., 12 (in comparison with the previous computational times). Due to these modifications, the computational performance of the DMRG-MRCI has presently proven to be approximately seven times faster than the previous implementation for the diferrate; the construction of a single σ-vector, which took approximately 10 days by means of the previous implementation, is now achievable in nearly 1 day.

The enhanced DMRG-cu(4)-MRCI methodology was applied to the determination of the stability of the iron(IV)-oxo porphyrin relative to the iron(V) electronic isomer (electromer) using the active space (29*e*,29*o*) (including four second d-shell orbitals of iron) with triple-ζ-quality atomic orbital basis sets. Based on the DMRG-cu(4)-MRCI+Q(PC) relative energies, the triradicaloid iron(IV)-oxo state was shown to be favored as the lowest energy state, and the iron(V) electromer was characterized as thermally inaccessible. This result is in accord with the earlier experimental and density functional studies. Contrarily, it conflicts with the previous RASPT2 (29*e*,28*o*) results reported by Pierloot et al.,[88] which showed that the hypothetical iron(V) state indicated by the recent LFP studies is located at low energy and thus likely to be thermally accessible (even with the account of solvent effects). Our DMRG-CASPT2 calculations predicted the low relative energy of the iron(V) electromer, basically confirming the previous RASPT2 and CASPT2 results. From the standpoint that the MRCI+Q model accounts for higher level dynamic correlation than the CASPT2 model (as illustrated in refs 78 and 155−157, for example), one could argue that the RASPT2, CASPT2, and DMRG-CASPT2 calculations all based on the second-order perturbation theory may too much overestimate the stability of the iron(V) electromer. Nonetheless, one should take into account the fact that the MRCI methods, even with the +Q correction, suffer from size-consistency errors, particularly for large systems, whereas the CASPT2/RASPT2 are almost a size-consistent theory. In our previous study, the DMRG-MRCI methods were numerically checked for free-base porphyrin, which can be viewed as a model system of FeO(P)Cl.[24] In addition, Shamasundar et al. presented various MRCI benchmarks for large systems using their efficient PIC-MRCI implementations. These studies should play a certain role in supporting the reliability of the present MRCI results; the concern with the size-consistency error could be addressed by MRCC-type theories,[31,32,77,78,158−173] whose applicability remains limited. We believe that what has been suggested by our DMRG-MRCI results is quite meaningful for shedding light on the details of the electronic nature of iron-oxo porphyrins. It should be further noted that the convergence of CAS with (29*e*,29*o*) remains elusive; therefore, the extension to the CAS should be tested for future work, for example, (a) inclusion of the other three N σ orbitals, (b) inclusion of the Cl's σ orbital, (c) inclusion of the fifth 3d′ orbital, (d) inclusion of the eight remote C's π orbitals, and (e) inclusion of the three lone pairs on Cl, etc.

■ ASSOCIATED CONTENT

Supporting Information

The Supporting Information is available free of charge on the ACS Publications website at DOI: 10.1021/acs.jctc.5b00270.

Natural orbitals obtained from the DMRG-CASSCF procedure (Figures S1−S3), the one-dimensional DMRG ordering of the localized MOs (Figure S4), and results of the check on the size-consistency errors of the DMRG-CASSCF and DMRG-MRCI methods for supersystems of polyene dimers (Tables SI and SII) (PDF)

■ AUTHOR INFORMATION

Corresponding Author

*E-mail: msaitow514@gmail.com.

Present Address

[‖]Max Planck Institute for Chemical Energy Conversion, Stiftstr. 3234, D-45470, Mülheim an der Ruhr, Germany.

Funding

Y.K. and T.Y. were supported by a Grant-in-Aid for Scientific Research (B) (Grant No. 25288013) and on Innovative Areas "Photosynergetics" (Grant No. 15H01097), and Y.K. also received funding by a Grant-in-Aid for Scientific Research (C) (Grant No. 25410030) and on Innovative Areas "Soft Molecular Systems" (Grant No. 26104538), from the Ministry of Education, Culture, Sports, Science and Technology-Japan (MEXT). Y.K. was supported by a grant of the Morino Foundation for Molecular Science.

Notes

The authors declare no competing financial interest.

■ ACKNOWLEDGMENTS

M.S. acknowledges Mr. Kantharuban Sivalingam for reading this manuscript and for giving informative comments. The generous support of computational resources from the Research Center of Computer Science (RCCS) at the Institute for Molecular Science (IMS) is acknowledged.

■ REFERENCES

(1) White, S. R. *Phys. Rev. Lett.* **1992**, *69*, 2863.
(2) White, S. R. *Phys. Rev. B: Condens. Matter Mater. Phys.* **1993**, *48*, 10345.
(3) White, S. R.; Martin, R. L. *J. Chem. Phys.* **1999**, *110*, 4127.
(4) Daul, S.; Ciofini, I.; Daul, C.; White, S. R. *Int. J. Quantum Chem.* **2000**, *79*, 331.
(5) Mitrushenkov, A. O.; Fano, G.; Ortolani, F.; Linguerri, R.; Palmieri, P. *J. Chem. Phys.* **2001**, *115*, 6815.
(6) Chan, G.-L.; Head-Gordon, M. *J. Chem. Phys.* **2002**, *116*, 4462.

DOI: 10.1021/acs.jctc.5b00270
J. Chem. Theory Comput. 2015, 11, 5120−5131

(7) Chan, G. K.-L.; Head-Gordon, M. *J. Chem. Phys.* **2003**, *118*, 8551.
(8) Chan, G. K.-L. *J. Chem. Phys.* **2004**, *120*, 3172.
(9) Ghosh, D.; Hachmann, J.; Yanai, T.; Chan, G. K.-L. *J. Chem. Phys.* **2008**, *128*, 144117.
(10) Chan, G.-L.; Dorando, J.; Ghosh, D.; Hachmann, J.; Neuscamman, E.; Wang, H.; Yanai, T. In *Frontiers in Quantum Systems in Chemistry and Physics*; Wilson, S., Grout, P., Delgado-Barrio, G., Maruani, J., Piecuch, P., Eds.; Progress in Theoretical Chemistry and Physics; Springer: Dordrecht, The Netherlands, 2008; Vol. *18*, pp 49−65.
(11) Chan, G. K.-L.; Zgid, D. *Annu. Rep. Comput. Chem.* **2009**, *5*, 149−162.
(12) Sharma, S.; Chan, G. K.-L. *J. Chem. Phys.* **2012**, *136*, 124121.
(13) Sharma, S.; Sivalingam, K.; Neese, F.; Chan, G. K.-L. *Nat. Chem.* **2014**, *6*, 927−933.
(14) Zgid, D.; Nooijen, M. *J. Chem. Phys.* **2008**, *128*, 014107.
(15) Zgid, D.; Nooijen, M. *J. Chem. Phys.* **2008**, *128*, 144115.
(16) Zgid, D.; Nooijen, M. *J. Chem. Phys.* **2008**, *128*, 144116.
(17) Legeza, Ö; Röder, J.; Hess, B. A. *Phys. Rev. B: Condens. Matter Mater. Phys.* **2003**, *67*, 125114.
(18) Moritz, G.; Hess, B. A.; Reiher, M. *J. Chem. Phys.* **2005**, *122*, 024107.
(19) Marti, K. H.; Ondík, I. M.; Moritz, G.; Reiher, M. *J. Chem. Phys.* **2008**, *128*, 014104.
(20) Marti, K. H.; Reiher, M. *Phys. Chem. Chem. Phys.* **2011**, *13*, 6750−6759.
(21) Podewitz, M.; Stiebritz, M. T.; Reiher, M. *Faraday Discuss.* **2011**, *148*, 119−135.
(22) Kurashige, Y.; Yanai, T. *J. Chem. Phys.* **2009**, *130*, 234114.
(23) Kurashige, Y.; Yanai, T. *J. Chem. Phys.* **2011**, *135*, 094104.
(24) Saitow, M.; Kurashige, Y.; Yanai, T. *J. Chem. Phys.* **2013**, *139*, 044118.
(25) Kurashige, Y.; Chan, G.; Yanai, T. *Nat. Chem.* **2013**, *5*, 660−666.
(26) Lan, T. N.; Kurashige, Y.; Yanai, T. *J. Chem. Theory Comput.* **2014**, *10*, 1953.
(27) Kurashige, Y. *Mol. Phys.* **2014**, *112*, 1485−1494.
(28) Nguyen Lan, T.; Kurashige, Y.; Yanai, T. *J. Chem. Theory Comput.* **2015**, *11*, 73−81.
(29) Kurashige, Y.; Chalupskỳ, J.; Lan, T. N.; Yanai, T. *J. Chem. Phys.* **2014**, *141*, 174111.
(30) Chalupskỳ, J.; Rokob, T. A.; Kurashige, Y.; Yanai, T.; Solomon, E. I.; Rulisek, L.; Srnec, M. *J. Am. Chem. Soc.* **2014**, *136*, 15977−15991.
(31) Neuscamman, E.; Yanai, T.; Chan, G. K.-L. *J. Chem. Phys.* **2010**, *132*, 024106.
(32) Yanai, T.; Kurashige, Y.; Neuscamman, E.; Chan, G. K.-L. *J. Chem. Phys.* **2010**, *132*, 024105.
(33) Ma, Y.; Ma, H. *J. Chem. Phys.* **2013**, *138*, 224105.
(34) Wouters, S.; Poelmans, W.; Ayers, P. W.; Van Neck, D. *Comput. Phys. Commun.* **2014**, *185*, 1501−1514.
(35) Wouters, S.; Nakatani, N.; Van Neck, D.; Chan, G. K.-L. *Phys. Rev. B: Condens. Matter Mater. Phys.* **2013**, *88*, 075122.
(36) Wouters, S.; Bogaerts, T.; Van der Voort, P.; Van Speybroeck, V.; Van Neck, D. *J. Chem. Phys.* **2014**, *140*, 241103.
(37) Wouters, S.; Van Neck, D. *Eur. Phys. J. D* **2014**, *68*, 272.
(38) Sharma, S.; Chan, G. K.-L. *J. Chem. Phys.* **2014**, *141*, 111101.
(39) Sharma, S. *J. Chem. Phys.* **2015**, *142*, 024107.
(40) Parker, S. M.; Shiozaki, T. *J. Chem. Phys.* **2014**, *141*, 211102.
(41) Chan, G. K.-L.; Sharma, S. *Annu. Rev. Phys. Chem.* **2011**, *62*, 465−481.
(42) SchollwÖck, U. *Rev. Mod. Phys.* **2005**, *77*, 259.
(43) SchollwÖck, U. *Ann. Phys.* **2011**, *326*, 96−192.
(44) Östlund, S.; Rommer, S. *Phys. Rev. Lett.* **1995**, *75*, 3537−3540.
(45) Rommer, S.; Östlund, S. *Phys. Rev. B: Condens. Matter Mater. Phys.* **1997**, *55*, 2164−2181.
(46) Verstraete, F.; Porras, D.; Cirac, J. I. *Phys. Rev. Lett.* **2004**, *93*, 227205.
(47) Roos, B. O. *Adv. Chem. Phys.* **1987**, *69*, 399.
(48) Ruedenberg, K.; Schmidt, M. W.; Gilbert, M. M.; Elbert, S. T. *Chem. Phys.* **1982**, *71*, 41.
(49) Buenker, R. J.; Peyerimhoff, S. D. *Theor. Chim. Acta.* **1974**, *35*, 33.
(50) Buenker, R. J.; Peyerimhoff, S. D. *Theor. Chim. Acta.* **1975**, *39*, 217.
(51) Lischka, H.; Shepard, R.; Pitzer, R. M.; Shavitt, I.; Dallos, M.; Müller, T.; Szalay, P. G.; Seth, M.; Kedziora, G. S.; Yabushita, S.; Zhang, Z. *Phys. Chem. Chem. Phys.* **2001**, *3*, 664.
(52) Lischka, H.; Müller, T.; Szalay, P. G.; Shavitt, I.; Pitzer, R. M.; Shepard, R. *WIREs. Comput. Mol. Sci.* **2011**, *1*, 191.
(53) Szalay, P. G.; Müller, T.; Gidofalvi, G.; Lischka, H.; Shepard, R. *Chem. Rev.* **2012**, *112*, 108.
(54) Venkatnathan, A.; Szilva, A. B.; Walter, D.; Gdanitz, R. J.; Carter, E. A. *J. Chem. Phys.* **2004**, *120*, 1693.
(55) Krisiloff, D. B.; Carter, E. A. *Phys. Chem. Chem. Phys.* **2012**, *14*, 7710.
(56) Werner, H.-J.; Reinsch, E.-A. *J. Chem. Phys.* **1982**, *76*, 3144.
(57) Werner, H.-J.; Knowles, P. J. *J. Chem. Phys.* **1988**, *89*, 5803.
(58) Knowles, P. J.; Werner, H.-J. *Chem. Phys. Lett.* **1988**, *145*, 514.
(59) Shamasundar, K. R.; Knizia, G.; Werner, H.-J. *J. Chem. Phys.* **2011**, *135*, 054101.
(60) Shiozaki, T.; Knizia, G.; Werner, H.-J. *J. Chem. Phys.* **2011**, *134*, 034113.
(61) Shiozaki, T.; Werner, H.-J. *J. Chem. Phys.* **2011**, *134*, 184104.
(62) Neese, F. *J. Chem. Phys.* **2003**, *119*, 9428.
(63) Hanrath, M.; Engels, B. *Chem. Phys.* **1997**, *225*, 197.
(64) Langhoff, S. R.; Davidson, E. R. *Int. J. Quantum Chem.* **1974**, *8*, 61.
(65) Davidson, E. R.; Silver, D. W. *Chem. Phys. Lett.* **1977**, *52*, 403.
(66) Pople, J. A.; Seeger, R.; Krishnan, R. *Int. J. Quantum Chem.* **1977**, *12* (S11), 149.
(67) Gdanitz, R.; Ahlrichs, R. *Chem. Phys. Lett.* **1988**, *143*, 413.
(68) Gdanitz, R. *Int. J. Quantum Chem.* **2001**, *85*, 281.
(69) Cardoen, W.; Gdanitz, R. *Chem. Phys. Lett.* **2002**, *364*, 39.
(70) Szalay, P. G.; Bartlett, R. J. *Chem. Phys. Lett.* **1993**, *214*, 481.
(71) Füsti-Molnár, L.; Szalay, P. G. *J. Phys. Chem.* **1996**, *100*, 6288.
(72) Szalay, P. G. *Chem. Phys.* **2008**, *349*, 121.
(73) Szalay, P. G.; Müller, T.; Lischka, H. *Phys. Chem. Chem. Phys.* **2000**, *2*, 2067.
(74) Andersson, K.; Malmqvist, P.-Å; Roos, B. O.; Sadlej, A. J.; Wolinski, K. *J. Phys. Chem.* **1990**, *94*, 5483−5488.
(75) Andersson, K.; Malmqvist, P.-Å; Roos, B. O. *J. Chem. Phys.* **1992**, *96*, 1218.
(76) Nakano, H. *J. Chem. Phys.* **1993**, *99*, 7983.
(77) Yanai, T.; Chan, G. K.-L. *J. Chem. Phys.* **2006**, *124*, 194106.
(78) Yanai, T.; Chan, G. K.-L. *J. Chem. Phys.* **2007**, *127*, 104107.
(79) Meyer, W. In *Methods of Electronic Structure Theory*, Modern Theoretical Chemistry, Vol. *3*; Schaefer, H. F., III, Eds.; Plenum: New York, 1977; DOI: 10.1007/978-1-4757-0887-5_11.
(80) Meyer, W. *J. Chem. Phys.* **1976**, *64*, 2901.
(81) Pulay, P.; Saebø, S.; Meyer, W. *J. Chem. Phys.* **1984**, *81*, 1901.
(82) Siegbahn, P. E. M.; Svensson, M. *Int. J. Quantum Chem.* **1992**, *41*, 153.
(83) MacLeod, M. K.; Shiozaki, T. *J. Chem. Phys.* **2015**, *142*, 051103.
(84) Shaik, S.; Kumar, D.; de Visser, S.; Altun, A.; Thiel, W. *Chem. Rev.* **2005**, *105*, 2279−2328.
(85) Altun, A.; Kumar, D.; Neese, F.; Thiel, W. *J. Phys. Chem. A* **2008**, *112*, 12904−12910.
(86) Chen, H.; Song, J.; Lai, W.; Wu, W.; Shaik, S. *J. Chem. Theory Comput.* **2010**, *6*, 940−953.
(87) Chen, H.; Lai, W.; Shaik, S. *J. Phys. Chem. B* **2011**, *115*, 1727−1742.
(88) Radoń, M.; Broclawik, E.; Pierloot, K. *J. Chem. Theory Comput.* **2011**, *7*, 898.
(89) Davidson, E. R. *J. Comput. Phys.* **1975**, *17*, 87.
(90) Liu, B. *Numerical Algorithms in Chemistry: Algebraic Methods*, Report on the Workshop; Lawrence Berkeley Laboratory, University of California: Berkeley, CA, USA, 1978.
(91) Kutzelnigg, W.; Mukherjee, D. *J. Chem. Phys.* **1997**, *107*, 432.
(92) Janssen, C. L.; Schaefer, H. F. *Theor. Chim. Acta.* **1991**, *79*, 1.

DOI: 10.1021/acs.jctc.5b00270
J. Chem. Theory Comput. 2015, 11, 5120−5131

(93) Neuscamman, E.; Yanai, T.; Chan, G. K.-L. *J. Chem. Phys.* **2009**, *130*, 124102.
(94) Neuscamman, E.; Yanai, T.; Chan, G. K.-L. *J. Chem. Phys.* **2009**, *130*, 169901.
(95) Neuscamman, E.; Yanai, T.; Chan, G. K.-L. *Int. Rev. Phys. Chem.* **2010**, *29*, 231.
(96) Saitow, M. *FEMTO:: An Integrated Toolset for the Automated Tensor Generation*, Version 0.1.0, https://github.com/msaitow, accessed Sep. 17, 2015.
(97) Hanrath, M.; Engels-Putzka, A. *J. Chem. Phys.* **2010**, *133*, 064108.
(98) Engels-Putzka, A.; Hanrath, M. *J. Chem. Phys.* **2011**, *134*, 124106.
(99) Hirata, S. *J. Phys. Chem. A* **2003**, *107*, 9887.
(100) Hanauer, M.; Köhn, A. *J. Chem. Phys.* **2011**, *134*, 204111.
(101) Auer, A. A.; Baumgartner, G.; Bernholdt, D. E.; Bibireata, A.; Choppella, V.; Cociorva, D.; Gao, X.; Harrison, R.; Krishnamoorthy, S.; Krishnan, S.; Lam, C.-C.; Lu, Q.; Nooijen, M.; Pitzer, R.; Ramanujam, J.; Sadayappan, P.; Sibiryakov, A. *Mol. Phys.* **2006**, *104*, 211−228.
(102) Angeli, C.; Cimiraglia, R.; Evangelisti, S.; Leininger, T.; Malrieu, J. P. *J. Chem. Phys.* **2001**, *114*, 10252.
(103) Angeli, C.; Cimiraglia, R.; Pastore, M. A comparison of various approaches in internally contracted multireference configuration interaction: the carbon dimer as a test case. *Mol. Phys.* **2012**, *110* (23), 2963−2968.
(104) Colmenero, F.; Pérez del Valle, C.; Valdemoro, C. *Phys. Rev. A: At., Mol., Opt. Phys.* **1993**, *47*, 971.
(105) Colmenero, F.; Valdemoro, C. *Phys. Rev. A: At., Mol., Opt. Phys.* **1993**, *47*, 979.
(106) Shamasundar, K. R. *J. Chem. Phys.* **2009**, *131*, 174109.
(107) Kutzelnigg, W.; Shamasundar, K. R.; Mukherjee, D. *Mol. Phys.* **2010**, *108*, 433.
(108) Hanauer, M.; Köhn, A. *Chem. Phys.* **2012**, *401*, 50.
(109) *The Haskell Programming Language*, http://www.haskell.org/.
(110) In case of the tensor-contracted term with five factors, the number of unique ways to construct the binary contraction increases to 105(!). For the term with the arbitrary number of the tensor factors, a sophisticated algorithm to form the binary contraction and to factorize the common intermediate tensor is developed on the basis of the binary-tree data structure. Because of the recursive nature of this, the algorithm can be implemented straightforwardly by using the functional programming language. This will be described in detail elsewhere.
(111) *Haskell in industry*, https://wiki.haskell.org/Haskell_in_industry, accessed Sep. 17, 2015.
(112) Kurashige, Y.; Saitow, M.; Chalupský, J.; Yanai, T. *Phys. Chem. Chem. Phys.* **2014**, *16*, 11988.
(113) Celani, P.; Werner, H.-J. *J. Chem. Phys.* **2000**, *112*, 5546.
(114) Celani, P.; Werner, H.-J. *J. Chem. Phys.* **2003**, *119*, 5044.
(115) Werner, H.-J.; Knowles, P. J.; Knizia, G.; Manby, F. R.; Schütz, M. *WIREs. Comput. Mol. Sci.* **2012**, *2*, 242.
(116) Jung, C. *Biochim. Biophys. Acta, Proteins Proteomics* **2011**, *1814*, 46−57.
(117) Ortiz de Montellano, P. R. *Cytochrome P450: Structure, Mechanism, and Biochemistry*, 3rd ed.; Kluwer Academic/Plenum: New York, 2005.
(118) Pan, Z.; Zhang, R.; Newcomb, M. *J. Inorg. Biochem.* **2006**, *100*, 524−532.
(119) Gold, A.; Weiss, R. *J. Porphyrins Phthalocyanines* **2000**, *4*, 344.
(120) Weiss, R.; Bulach, V.; Gold, A.; Terner, J.; Trautwein, A. X. *JBIC, J. Biol. Inorg. Chem.* **2001**, *6*, 831.
(121) Groves, J. T. *J. Inorg. Biochem.* **2006**, *100*, 434.
(122) Kim, S. H.; Perera, R.; Hager, L. P.; Dawson, J. H.; Hoffman, B. M. *J. Am. Chem. Soc.* **2006**, *128*, 5598.
(123) Nam, W. *Acc. Chem. Res.* **2007**, *40*, 522.
(124) Rittle, J.; Green, M. T. *Science* **2010**, *330*, 933.
(125) Yamaguchi, K.; Watanabe, Y.; Morishima, I. *J. Chem. Soc., Chem. Commun.* **1992**, 1721.
(126) Murakami, T.; Yamaguchi, K.; Watanabe, Y.; Morishima, I. *Bull. Chem. Soc. Jpn.* **1998**, *71*, 1343.
(127) Harischandra, D.; Lowery, G.; Zhang, R.; Newcomb, M. *Org. Lett.* **2009**, *11*, 2089−2092.
(128) de Oliveira, F. T.; Chanda, A.; Banerjee, D.; Shan, X.; Mondal, S.; Que, L.; Bominaar, E. L.; Münck, E.; Collins, T. J. *Science* **2007**, *315*, 835−838.
(129) Lee, S.; Han, J.; Kwak, H.; Lee, S.; Lee, E.; Kim, H.; Lee, J.; Bae, C.; Lee, S.; Kim, Y.; Kim, C. *Chem. - Eur. J.* **2007**, *13*, 9393−9398.
(130) Pan, Z.; Wang, Q.; Sheng, X.; Horner, J.; Newcomb, M. *J. Am. Chem. Soc.* **2009**, *131*, 2621−2628.
(131) Malmqvist, P.-Å; Pierloot, K.; Rehaman, A.; Shahi, M.; Cramer, C. J.; Gagliardi, L. *J. Chem. Phys.* **2008**, *128*, 204109.
(132) Roos, B. O.; Taylor, P. R.; Siegbahn, P. E. *Chem. Phys.* **1980**, *48*, 157.
(133) Roos, B. O. *Adv. Chem. Phys.* **1987**, *69*, 399.
(134) Ruedenberg, K.; Cheung, L. M.; Elbert, S. T. *Int. J. Quantum Chem.* **1979**, *16*, 1069.
(135) Olsen, J.; Roos, B. O.; Jørgensen, P.; Jensen, H. J. Aa. *J. Chem. Phys.* **1988**, *89*, 2185.
(136) Malmqvist, P.-Å; Rendell, A.; Roos, B. O. *J. Phys. Chem.* **1990**, *94*, 5477.
(137) Nakano, H.; Uchiyama, R.; Hirao, K. *J. Comput. Chem.* **2002**, *23*, 1166.
(138) Walter, D.; Carter, E. A. *Chem. Phys. Lett.* **2001**, *346*, 177.
(139) Faglioni, F.; Goddard, W. *Int. J. Quantum Chem.* **1999**, *73*, 1.
(140) Hunt, W. J.; Hay, P. J.; Goddard, W. A., III. *J. Chem. Phys.* **1972**, *57*, 738.
(141) Cullen, J. *Chem. Phys.* **1996**, *202*, 217.
(142) Van Voorhis, T.; Head-Gordon, M. *J. Chem. Phys.* **2002**, *117*, 9190.
(143) Rassolov, V. A.; Xu, F. *J. Chem. Phys.* **2007**, *127*, 044104.
(144) Parkhill, J. A.; Lawler, K.; Head-Gordon, M. *J. Chem. Phys.* **2009**, *130*, 084101.
(145) Li Manni, G.; Ma, D.; Aquilante, F.; Olsen, J.; Gagliardi, L. *J. Chem. Theory Comput.* **2013**, *9*, 3375−3384.
(146) Ivanic, J. *J. Chem. Phys.* **2003**, *119*, 9364−9376.
(147) Parker, S. M.; Seideman, T.; Ratner, M. A.; Shiozaki, T. *J. Chem. Phys.* **2013**, *139*, 021108.
(148) Becke, A. D. *Phys. Rev. A: At., Mol., Opt. Phys.* **1988**, *38*, 3098−3100.
(149) Perdew, J. P. *Phys. Rev. B: Condens. Matter Mater. Phys.* **1986**, *33*, 8822−8824.
(150) Roos, B.; Lindh, R.; Malmqvist, P.; Veryazov, V.; Widmark, P. *J. Phys. Chem. A* **2005**, *109*, 6575−6579.
(151) Douglas, M.; Kroll, N. M. *Ann. Phys. (Amsterdam, Neth.)* **1974**, *82*, 89−155.
(152) Heß, B. A. *Phys. Rev. A: At., Mol., Opt. Phys.* **1986**, *33*, 3742−3748;Jansen, G.; Heß, B. A. *Phys. Rev. A: At., Mol., Opt. Phys.* **1989**, *39*, 6016−6017.
(153) Ghigo, G.; Roos, B. O.; Malmqvist, P.-Å. *Chem. Phys. Lett.* **2004**, *396*, 142.
(154) Forsberg, N.; Malmqvist, P.-Å. *Chem. Phys. Lett.* **1997**, *274*, 196−204.
(155) Shiozaki, T.; Mizukami, W. *J. Chem. Theory Comput.* **2015**, DOI: 10.1021/acs.jctc.5b00754.
(156) Neuscamman, E. *J. Chem. Phys.* **2013**, *139*, 181101.
(157) Cabrero, J.; Caballol, R.; Malrieu, J.-P. *Mol. Phys.* **2002**, *100*, 919−926.
(158) Mukherjee, D.; Moitra, R. K.; Mukhopadhyay, A. *Mol. Phys.* **1977**, *33*, 955.
(159) Jeziorski, B.; Monkhorst, H. J. *Phys. Rev. A: At., Mol., Opt. Phys.* **1981**, *24*, 1668.
(160) Mahapatra, U. S.; Datta, B.; Mukherjee, D. *Mol. Phys.* **1998**, *94*, 157.
(161) Hanrath, M. *J. Chem. Phys.* **2005**, *123*, 084102.
(162) Banerjee, A.; Simons, J. *Int. J. Quantum Chem.* **1981**, *19*, 207.
(163) Laidig, W. D.; Saxe, P.; Bartlett, R. J. *J. Chem. Phys.* **1987**, *86*, 887.

DOI: 10.1021/acs.jctc.5b00270
J. Chem. Theory Comput. 2015, 11, 5120−5131

(164) Hanauer, M.; Köhn, A. *J. Chem. Phys.* **2012**, *137*, 131103.
(165) Hanauer, M.; Köhn, A. *J. Chem. Phys.* **2012**, *136*, 204107.
(166) Evangelista, F.; Hanauer, M.; Köhn, A.; Gauss, J. *J. Chem. Phys.* **2012**, *136*, 204108.
(167) Evangelista, F.; Gauss, J. *J. Chem. Phys.* **2011**, *134*, 114102.
(168) Jagau, T.-C.; Prochnow, E.; Evangelista, F.; Gauss, J. *J. Chem. Phys.* **2010**, *132*, 144110.
(169) Jagau, T.-C.; Gauss, J. *Chem. Phys.* **2012**, *401*, 73.
(170) Jagau, T.-C.; Gauss, J. *J. Chem. Phys.* **2012**, *137*, 044115.
(171) Jagau, T.-C.; Gauss, J. *J. Chem. Phys.* **2012**, *137*, 044116.
(172) Ivanov, V. V.; Adamowicz, L. *J. Chem. Phys.* **2000**, *112*, 9258.
(173) Datta, D.; Kong, L.; Nooijen, M. *J. Chem. Phys.* **2011**, *134*, 214116.

DOI: 10.1021/acs.jctc.5b00270
J. Chem. Theory Comput. 2015, 11, 5120−5131